

# PCCP

Accepted Manuscript



This is an *Accepted Manuscript*, which has been through the Royal Society of Chemistry peer review process and has been accepted for publication.

*Accepted Manuscripts* are published online shortly after acceptance, before technical editing, formatting and proof reading. Using this free service, authors can make their results available to the community, in citable form, before we publish the edited article. We will replace this *Accepted Manuscript* with the edited and formatted *Advance Article* as soon as it is available.

You can find more information about *Accepted Manuscripts* in the [Information for Authors](#).

Please note that technical editing may introduce minor changes to the text and/or graphics, which may alter content. The journal's standard [Terms & Conditions](#) and the [Ethical guidelines](#) still apply. In no event shall the Royal Society of Chemistry be held responsible for any errors or omissions in this *Accepted Manuscript* or any consequences arising from the use of any information it contains.

# Photoisomerisation of azobenzene crystals in aqueous dispersions examined by higher order derivative spectra

Cite this: DOI: 10.1039/x0xx00000x

Kunihiro Ichimura

Received 00th January 2012,  
Accepted 00th January 2012

DOI: 10.1039/x0xx00000x

www.rsc.org/

Photo-induced UV-VIS spectral changes of azobenzene (Az) in solutions and aqueous crystalline dispersions were analysed by means predominantly of the fourth order derivatives. Weak bands due to vibration level transitions (VLT) of *E*-isomers in solution were well resolved in derivatives to estimate conversions of photoisomerisation by tracing extrema of a VLT sub-peak. The photo-induced derivative-spectral changes of Az crystals dispersed in aqueous PVA solutions generated many common crossing points to indicate that Az dissolves partially in a PVA solution to lead to the photoisomerisation in a homogeneous phase and the reversible alteration of particle sizes. The solid-state photoisomerisation of Az was investigated by the preparation of PVA-free aqueous dispersions of powdery nanohybrids comprised of Az and silica nanoparticles. The fourth order derivatives of spectral changes revealed that the photochemical process involves three kinds of species including non-aggregated and aggregated *E*-isomer as well as *Z*-isomer.

## Introduction

Photochemical changes of molecules or residues embedded in various types of photofunctional materials are primarily followed by UV-VIS spectral measurements. This approach is encountered by difficulties in many cases to achieve quantitative and even qualitative analyses because of the followings. The conventional approach is carried out in such a way that UV-VIS spectral changes of a model compound under photoirradiation have been used to be taken in a transparent and dilute solution. UV-VIS spectra of the same chromophore incorporated in photofunctional materials suffer from the transformation of spectral shapes more or less owing to effects of matrices, as stated below. Accordingly, we can do nothing but extract occasionally photosensitive molecules from matrices by means of an appropriate procedure in a destructive way to estimate the photochemistry occurring in the materials. The purpose of this work aims at demonstrating the significance of higher order derivative UV-VIS spectra, presupposing the non-destructive analysis of photofunctional materials. The geometrical photoisomerisation of azobenzene (Az) in solution, aqueous dispersions in poly(alcohol alcohol) (PVA) solution and aqueous PVA-free dispersions of Az crystals is used here because the chemistry consists solely of two *E*- and *Z*-isomers.<sup>1</sup>

The photoisomerisation and thermal reversion of Az and the related compounds has been extensively studied owing to the reversibility with reasonable quantum yields and excellent photofatigue resistance. The fundamental studies on photochemistry and photophysics of Az and the like are tightly linked with applicabilities to versatile photofunctional materials owing to tailor-made molecular design as well as straightforward changes in molecular shape and dipole moment.<sup>1,2</sup> Accordingly, light-triggered molecular systems have been developed to exhibit the photoswitching of optical, electrical, mechanical and magnetical properties as well as chemical and biological performances.<sup>3</sup> The rod-like shape of *E*-

azobenzene is equivalent to mesogen so that this type of chromophores plays crucial roles in photo-induced mesophase changes, surface-mediated liquid crystals (LC) photoalignment,<sup>4</sup> photomechanical movement,<sup>5</sup> surface relief grating formation,<sup>6</sup> erasable photomemories derived from LC polymers<sup>7</sup> and so on. The reversible modification of dipole moment leads, for instance, versatile changes in the sedimentation of Az molecules<sup>8</sup> as well as particles surface-modified with Az.<sup>9</sup> Az chromophores have been embedded in organic, inorganic and even organic-inorganic hybridised materials in homogeneous as well as heterogeneous circumstances to fabricate versatile types of photo-triggered materials.

Measurements of UV-VIS absorption spectra of Az-modified photoresponsive materials have so far been carried out routinely to discuss the photofunctionality. For instance, the emergence of isosbestic point(s) in spectral changes under UV-VIS light irradiation has been pointed out to claim the reversibility of photoisomerisation. But care should be taken in achieving such approach for quantitative discussions. There is the possibility to form aggregate(s) due to the local condensation of Az and the related units incorporated in photofunctional solid or fluid matrices. Furthermore, the photo-induced modulation of the interplay between Az units and matrices should perturb UV-VIS spectral changes more or less. It is needed to remind consequently that UV-VIS spectral changes are based not only on the photoisomerisation of monomeric Az unit, but also on the photo-induced modification of molecular interactions of Az in photoresponsive systems so that spectral changes may deviate from isosbestic point(s). Besides, no isosbestic point is available sometimes because of the absorption and/or scattering of light by matrices. ED (extinction difference)- as well as EDQ (extinction quotient difference)-diagram analyses have been achieved sometimes for such systems to confirm the single process,<sup>10</sup> assuming that the system consist solely of two monomeric isomers.

Accordingly, strictly speaking, the analyses of photoresponsive materials by ED- and EDQ-diagram include the restriction because of the situations discussed just above.

Meanwhile, derivative spectra have been used extensively, in particular, for qualitative as well as quantitative analyses predominantly in pharmaceutical, biological and clinical researches because they possess the following features.<sup>11</sup> First, the Beer's law is maintained in every derivative spectrum so that quantitative analysis is possible. Secondly, the sharpening of signals is attained in higher order derivatives so that even weak shoulders become resolved, and closely overlapped bands are sufficiently separated. Thirdly, linear background coming from light scattering is effectively eliminated to enable us to analyse turbid samples purposively. Note that samples for pharmaceutical, biological and clinical researches are principally water-borne so that UV-VIS spectra are basically taken for dispersions in water or solid matrices. This situation implies the practical significance of UV-VIS derivative spectra of versatile photoresponsive materials to elucidate photochemical events in heterogeneous systems. Nevertheless, the usefulness of derivative spectra in researches of photofunctional materials has not been stressed systematically except for our recent works,<sup>12-14</sup> to the author's knowledge, whereas lower (first or second) derivative spectra have been sporadically reported to determine  $\lambda_{max}$  or to discuss the position of aggregated species of photosensitive polymers.

We reported that higher order derivative spectra of two types of photodimerisable polymers in solutions and transparent films to identify aggregated species acting as photocrosslinking units.<sup>12,13</sup> Higher order derivative spectra of water-soluble poly(vinyl alcohols) with styrylpyridinium side chains (PVA-SbQ) in aqueous solutions and films disclosed the presence of H-aggregate, which photodimerises quite rapidly when compared with non-aggregated SbQ.<sup>12</sup> The derivatives were also applied to elucidate the photocrosslinking behaviour of a turbid film prepared from a mixture of PVA-SbQ and an aqueous polymer emulsion, which have been used extensively for making stencils for screen printing. Higher order derivative spectra of hyper-branched polycinnamates disclosed also that cinnamate side chains form J-aggregate, which photodimerises very quickly.<sup>13</sup> Encouraged by the results, the same approach has been made to reveal the individual photoreorientation of H- and J-aggregated azobenzene side chains attached an LC polymer in transparent films under irradiation with linearly polarised light.<sup>14</sup>

In this work, the trivial photoisomerisation of Az in dilute solution will be treated at first as a model system to depict the fundamental procedure and the significance of derivative-spectral analysis. Subsequently, the photochemical behaviour of mechanically milled dispersions of Az crystals in aqueous PVA solutions and dispersions of powdery nanohybrids of Az and silica nanoparticles in PVA-free water will be mentioned as heterogeneous systems.<sup>15</sup>

## Results and discussion

### Dilute solution of Az

Fig. 1a shows well-known changes in absorption spectra of Az in dilute cyclohexane solution upon exposure to 313 nm with use of a diode array spectrometer at the 1 nm spacing. The  $\pi, \pi^*$ -band exhibits the fine structure with four weak shoulders, while clear-cut isosbestic points emerge upon photoirradiation. This is a trivial event. The spectral changes were subsequently converted into second, fourth and eighth order derivatives after the optimised spectral smoothing according to the Savitzky-Golay algorithm as described in our previous reports.<sup>12,13</sup> The results are given in Figs. 1b, 1c and 1d,

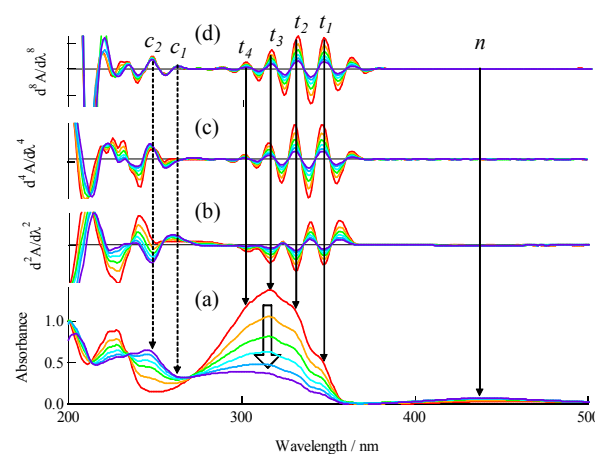


Fig. 1 Changes in (a) absorption spectra and (b) the second, (c) fourth and (d) eighth derivative spectra of a dilute hexane solution upon exposure to 313 nm light.

respectively. Notice that extrema in the second derivatives appear at the minima while those in the fourth and eighth order derivative at maxima. The extremum values of the second, fourth and eighth derivatives are denoted as  $d^2$ ,  $d^4$  and  $d^8$ , respectively, throughout the text. The four shoulders of the  $\pi, \pi^*$ -band are converted into well-separated sub-peaks in the derivatives. The peak positions at 302 nm, 316 nm, 331 nm and 347 nm are practically identical in every derivative spectrum, implying that no sub-peak due to Z-isomer is present in this wavelength region. The peaks marked as  $t_1$ ,  $t_2$ ,  $t_3$  and  $t_4$  in Fig. 1 are separated at the same distance of  $\Delta E = 1430 \pm 40 \text{ cm}^{-1}$  within measurement errors. Note that the spacing of 1 nm is equivalent to that of  $60 \text{ cm}^{-1}$  so that the mean  $\Delta E$  value falls sufficiently within instrumental errors. Accordingly, the finely structured  $\pi, \pi^*$ -band consists of sub-peaks assignable to vibration level transition (VLT), just as in the cases of SbQ<sup>12</sup> and cinnamate<sup>13</sup> as linearly conjugated chromophores. It is worthy to mention that the maximum due to the  $n, \pi^*$ -band denoted as  $n$  in Fig. 1 is quite weak in every derivative spectrum. This is because the extremum value ( $d^n$ ) of the  $n$ -th order derivative is proportional to  $(1/W)^n$ , whereas  $W$  stands for a full width at half maximum. In other words, a sub-peak height  $d^n$  is extremely sensitive to  $W$ . Since the  $n, \pi^*$ -band with far lower absorption coefficient is much broader than the bands due to

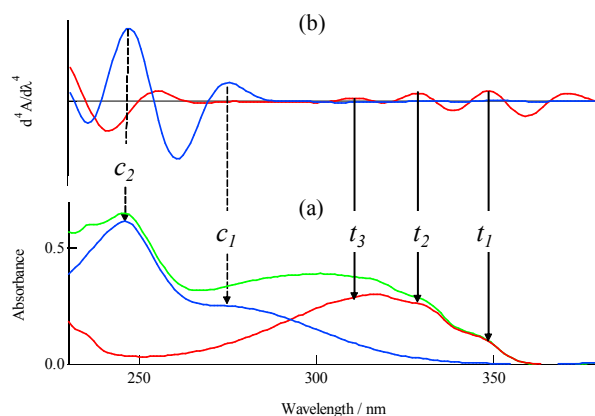


Fig. 2 (a) Absorption spectra and (b) the corresponding fourth order derivatives of Az at photostationary state upon exposure to 313 nm light in hexane (green line) and the calculated spectra of E- (red lines) and Z- isomer (blue lines) at the photostationary state.

VLT, the peak corresponding to the  $n, \pi^*$ -band in the derivatives becomes negligibly small. Accordingly,  $n, \pi^*$ -band plays essentially no role in the qualitative as well as quantitative analysis of Az photochemistry by derivative spectra. On the contrary, the VLT bands play a very crucial role in this study, whereas they have been attracting no interest for photochemical studies.

As seen in Fig. 1, the VLT sub-peaks of  $\pi, \pi^*$ -band decrease monotonously without any alteration of peak positions to reach to photostationary state. This fact suggests that the sub-peaks are not contaminated with those of *Z*-isomer, as mentioned above, to enable us to estimate levels of photoisomerisation simply by tracing changes in  $d^4$  values of Az, for instance, at 347 nm. Thus, a fraction of *E*-isomer under photoirradiation is conveniently estimated by  $d^4_i/d^4_0$ , whereas  $d^4_0$  and  $d^4_i$  are  $d^4$  values of a VLT sub-peak before and after photoirradiation. The alteration of *E*-isomer fraction during irradiation with 313 nm as well as 436 nm light can be conveniently followed by this procedure. For example, the contents of *E*-isomer at photostationary states upon prolonged exposure to 313 nm and 436 nm light were effortlessly estimated to be 22 % and 82 %, respectively. By using the levels of photoisomerisation thus estimated, the absorption spectrum after 313 nm light irradiation was separated into those of both isomers and shown in Fig. 2a. The calculated spectrum of *Z*-isomer was identical to that of isolated *Z*-isomer, and  $d^4$  values of *Z*-isomer are negligibly small at wavelengths longer than *ca.* 300 nm in line with the supposition stated above. The new sub-peak assignable to *Z*-isomer emerges at 273 nm (sub-peak  $c_1$ ) in the derivatives, whereas the observation of the peak is hard in Fig. 1 because  $d^4$  of the  $c_1$  peak is extremely small. Obviously, this situation comes from a broader width of 273 nm band, which possesses no VLT band owing to the flexible structure of the bend *Z*-isomer molecule.

In a system consisting of two components (*X* and *Y*),  $A_{\max}^X/A_{\text{iso}}$  or  $A_{\max}^Y/A_{\text{iso}}$  is proportional to fractions of *X* or *Y*, whereas  $A_{\text{iso}}$ ,  $A_{\max}^X$  and  $A_{\max}^Y$  are absorbances at an isobestic point and at  $\lambda_{\max}$  of *X* and *Y*, respectively. In order to verify the validity to estimate isomer fractions on the basis of derivative spectra,  $d^4/d^4_0$  values at 347 nm at every exposure dose were plotted against  $A_{316}/A_{271}$  values at the corresponding exposure doses, whereas  $A_{316}$  and  $A_{271}$  are absorbances at  $\lambda_{\max}$  of 316 nm of *E*-isomer and of the isobestic point at 271 nm, respectively. As shown in Fig. 3, good linearity was obtained, verifying the validity of the procedure to estimate *E*-fractions using the derivative spectra. Consequently, contents of *E*-isomer in photoirradiated samples are conveniently obtained by  $d^4/d^4_0$  values of a VLT sub-peak.

#### Dispersions of Az milled in aqueous PVA solutions

While Hartley described in 1937 that the *Z*-to-*E* isomerisation of Az occurs in crystals by exposure to strong sunlight,<sup>16</sup> there has been no unequivocal report on the *E*-to-*Z* photoisomerisation in crystalline state except for the AFM study on the photo-induced modification of crystal surface. It was suggested that a layered structure of Az crystal surface is reversibly transformed by UV and VIS light irradiation, leading to the conclusion that Az molecules in the topmost bilayers of crystals participate in photoisomerisation.<sup>17</sup> But no direct evidence for the photoisomerisation was presented except our preliminary reports.<sup>15</sup>

In order to observe the photoisomerisation directly with aid of

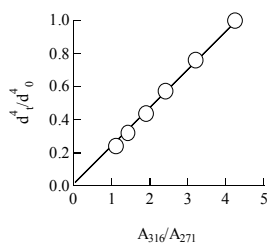


Fig. 3 Relation between  $d^4/d^4_0$  and  $A_{316}/A_{271}$ .

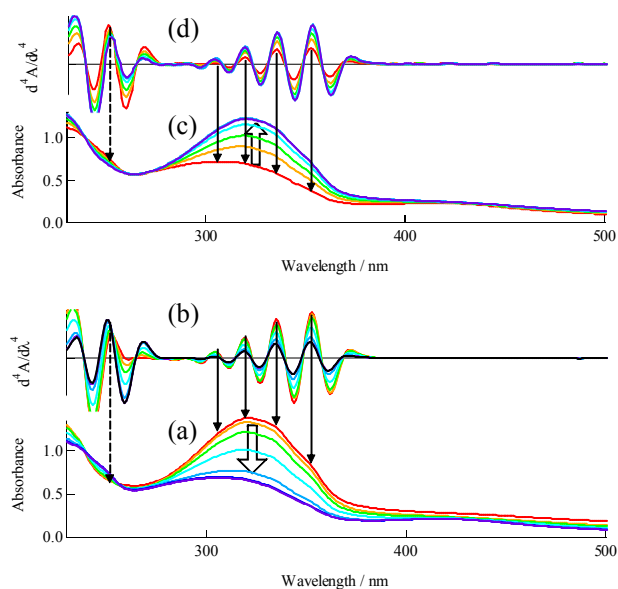


Fig. 4 Changes in absorption (a and c) and the corresponding fourth derivatives (b and d) of an aqueous dispersion of Az crystals beads-milled in a PVA solution upon exposure to 313 nm light (a and b) and subsequently to 436 nm light (c and d).

UV-VIS spectra, the downsizing of Az crystals may be purposive because of the enlargement of surface areas. This idea motivated us to perform the wet beads-milling of Az crystals in an aqueous solution of partially saponified PVA as a dispersion stabiliser with aid of fine zirconia beads to follow the solid-state photoisomerisation by means of UV-VIS spectra.<sup>15a</sup> The aqueous dispersions were subjected to centrifugation to remove crude particles, followed by photoirradiation under magnetic stirring to prevent the sedimentation of fine particles. Figs. 4a and 4c show the changes in absorption spectra under alternate irradiation with 313 nm and 436 nm light, respectively. Even though spectral shapes are affected by light scattering, isobestic points are apparently observed at the shorter wavelength region. The changes in fourth order derivatives for the forward and backward photoisomerisation are shown in Figs. 4b and 4d, respectively. Common crossing points are generated throughout the spectral ranges to confirm the photochemistry consisting of a single process. Four sub-peaks are observed in a manner similar to those in solution. The spectroscopic properties of Az in cyclohexane, methanol and the aqueous dispersion are compiled in Table 1.  $\Delta E$  in PVA dispersion is somewhat larger than that in solution. It is worthy to note that the red shift of  $\lambda_{\max}$  of  $\pi, \pi^*$ -band in an aqueous dispersion is indicative of the molecular dissolution of Az, which is hardly soluble in water.

Table 1 Spectroscopic properties

|                           | Cyclohexane | Methanol | Aq. dispersion |
|---------------------------|-------------|----------|----------------|
| $\lambda_{\max}$ / nm     | 316         | 317      | 320            |
|                           | 302         | 304      | 304            |
| sub-peak / nm             | 316         | 318      | 319            |
|                           | 331         | 333      | 335            |
|                           | 347         | 349      | 353            |
| $\Delta E/\text{cm}^{-1}$ | 1430±40     | 1410±40  | 1530±30        |

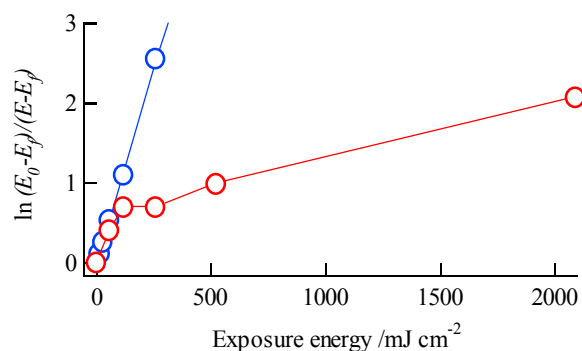


Fig. 5 The first order plots for *E-to-Z* photoisomerisation of Az in a hexane solution (blue circles) and in an aqueous PVA dispersion (red circles).

Thus, it is implied that the photoisomerisation is predominantly due to Az dissolved molecularly in a PVA solution.

The aqueous dispersions before and after exposure to 313 nm light were subjected to the extraction with hexane to take absorption spectra in solution. Levels of photoisomerisation in the dispersion were estimated by obtaining *E*-isomer fractions in hexane extracts by using  $d^t/d^t_0$  values of the VLT sub-peak at 347 nm according to the method mentioned above. Fig. 5 shows the first order plots for the *E-to-Z* photoisomerisation both in solution and in dispersion as a function of exposed UV-doses.  $E_0$  and  $E_f$  in the figure denote *E*-isomer fractions before and after prolonged photoirradiation of a 5.2 J cm<sup>-2</sup> dose, while  $E$  stands for *E*-isomer fractions at every exposure dose. The plots for the photoisomerisation in dispersion reveal evidently the involvement of two first order processes. The plots for the fast one deviate from a straight line at about a 100 mJ cm<sup>-2</sup> dose, followed by plots obeying very slow first order kinetics. The rate of the fast process is very close to that in cyclohexane and accordingly corresponds to the isomerisation of molecularly dissolved Az, while the subsequent slow process is reasonably assigned to the solid-state event. The dissolution of Az in aqueous PVA solution in a molecular level owes to the mechanical milling. The results reveal that the rate of the solid-state photoisomerisation is about one order magnitude slower than the solution photochemistry. We suggested in our preliminary report that the solid-state photoisomerisation of mill-dispersed Az on the basis of the changes in absorption spectra shown in Fig. 4,<sup>15a</sup> but this idea has to be corrected. Detailed discussion on the photoisomerisation specifically in crystalline state will be made below by employing Az/silica hybrid nanoparticles dispersed in PVA-free water.<sup>15b</sup>

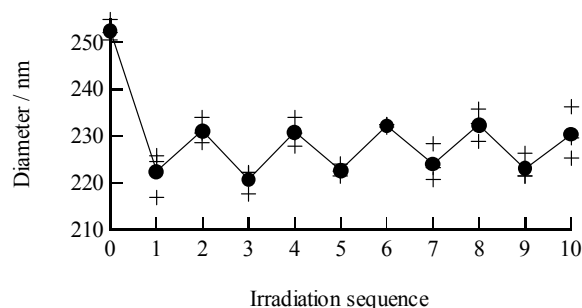


Fig. 6 Reversible changes in particle size of Az crystals dispersed in water upon alternate exposure to 313 nm (odd numbers) and 436 nm light (even numbers). Crosses and closed circles are observed and averaged values, respectively.

The other point to be referred in the spectral changes shown in Fig. 4a is the reversible alteration of baselines at the longer wavelength region. For instance, absorbances at about 500 nm decline upon irradiation with 313 nm light and increase under the subsequent irradiation with 436 nm light. Since  $d_4$  values at the longer wavelength region are negligibly small throughout the photoirradiation, this phenomenon is thought to come from the modification of light scattering. In other words, particle sizes of dispersed Az crystals are thought to be reversibly altered. This was the case, as shown in Fig. 6. Particle size measurements were performed for aqueous dispersions after alternate exposure to 313 nm and 436 nm light to give photostationary states. The particle size of a dispersion of 252±2 nm before photoirradiation was markedly reduced upon irradiation with 313 nm light, whereas the increment of particle size was observed after the subsequent 436 nm light irradiation. The changes in particle size distribution took place reversibly thereafter, and particle sizes upon exposure to 313 nm and 436 nm light were 223±1 nm and 231±1 nm, respectively. A ca. 3.5% volume change may be ascribable to the transformation between *E*-isomer with a rod-like shape and *Z*-isomer with a bent form. But it is hard to ascribe the volume change to the structural alteration of crystals, because the specific density of *E*-isomer<sup>18</sup> and *Z*-isomer<sup>19</sup> are 1.230 and 1.123, respectively, so that a crystal volume of *Z*-isomer should be rather slightly larger than that of *E*-isomer. Consequently, the particle size reduction by UV irradiation requires the another interpretation. There have been many reports on photoinduced volume changes of cast films of LC polymers<sup>20</sup> and stretched films of polymers substituted with Az units<sup>21</sup> to exhibit shrinkage due to *Z*-isomer formation. Two models have been proposed on the basis of the followings. The first is based on the geometrical shape change from linear *E*-form to bent *Z*-form to induce macroscopic size transformation, while the second stresses the attractive force due to the enhanced dipole moment of *Z*-isomer, resulting in the compaction of polymer chains. Whereas the former is thought to be associated with photoinduced phase changes of LC azo-polymer films, the latter has been proposed to interpret the reversible viscosity change of solutions of a poly(dimethylsiloxane) with azobenzene residues.<sup>22</sup> The former mechanism is not convincing for the present system, because Az molecules are not tethered covalently to PVA chains so that the molecular shape change of Az is insensible to polymer conformation. Therefore, the reversible alteration of particle size seems to be due to the second mechanism. Whereas PVA coils incorporating *E*-isomer molecules exhibit extended conformation, the conversion into *Z*-isomer leads to the shrinkage of PVA coils due to the dipole-dipole attractive force of *Z*-isomer, even though Az molecules are not covalently tethered to PVA chains.

As stated above, a fraction of *Z*-isomer at the photostationary state of the fast process is levelled off at ca. 14%. Since Az crystals weighing 150 mg were milled in 10.00 g of a 5 wt% of PVA solution in this experiment, dissolved Az molecules in PVA chains is estimated to be 18 (=14 ÷ 0.78) wt% of the fed crystals, assuming that the level of *E-to-Z* photoisomerisation is 78%. The PVA (GL-05) consists of vinyl alcohol and vinyl acetate as monomer units in a molar ratio of 0.88:0.12, so that an averaged molecular weight of monomer unit of GL-05 is 49.1. The number of Az molecules embedded in each PVA chain of polymerisation degree of 500 is 40 in average. Since each PVA chain possesses 60 vinyl acetate units, hydrophobic interactions between an Az molecule and vinyl acetate units together with methylene groups of vinyl alcohol units may work sufficiently.

#### Dispersions of Az/silica nanoparticles in aqueous solution of PVA

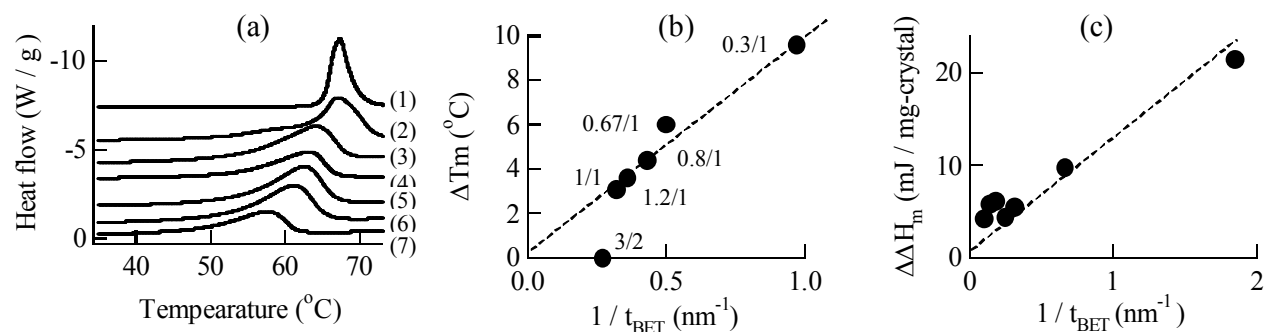


Fig. 7 (a) DSC 2nd heating scans of Az crystals and the Az/m-SiO<sub>2</sub> hybrids. From the top: (1) crystals, (2) 1.5/1 (w/w), (3) 1.2/1 (w/w), (4) 1/1 (w/w), (5) 0.8/1 (w/w), (6) 0.67/1 (w/w) and (7) 0.3/1 (w/w) hybrids. (b) Relationship between  $\Delta T_m$  and  $1/t_{BET}$  and (c) between  $\Delta\Delta H_m$  and  $1/t_{BET}$ .

We developed previously a novel method to fabricate powdery organic-inorganic nano hybrids of organic pigments<sup>23</sup> as well as molecular crystals<sup>24</sup> by means of the dry co-grinding with silica nanopowders. On the basis of transmission electron microscope (TEM) and energy-filtering (EF)-TEM measurements,<sup>25</sup> it was disclosed that the surface of silica powders, which consist of agglomerates of primary particles of a diameter of *ca.* 14 nm, is covered with ultrathin shell layers of organic crystals to give core-shell type nanostructures. Averaged diameters of primary particles of the hybrids are controllable by mixing ratios of organic crystals and silica nanoparticles. We anticipated that the dry grinding under controlled conditions causes the attrition of organic bulk crystals with silica nanoparticles, leading to the cohesion of crystalline nanofragments to build up shell layers onto hydrophobitised surfaces of silica nanoparticles.<sup>23,24a</sup> Interestingly, these kinds of hybrid powders are able to be dispersed in water even in absence of any surfactant. In this context, this technique is convenient to determine the solid-state photoisomerisation in aqueous phases in the presence as well as in absence of PVA.

Silica nanoparticles were treated in advance with a polysiloxane to cover surface silanols to prepare surface-modified silica nanoparticles (m-SiO<sub>2</sub>) for improving the affinity to hydrophobic organic crystals.<sup>23</sup> Voluminous powders prepared from a mixture of Az and m-SiO<sub>2</sub> in 1 : n in weight are hereafter denoted as AzH-n. A BET (Brunauer-Emmett-Teller) specific surface area ( $S_{BET}$ ) of m-

SiO<sub>2</sub> was 152.6 m<sup>2</sup>/g. The nano hybridisation led to the reduction of  $S_{BET}$  values, and  $S_{BET}$  of AzH-1, AzH-0.3 and AzH-0.1 were 79.6 m<sup>2</sup>/g, 123.6 m<sup>2</sup>/g and 139.8 m<sup>2</sup>/g, respectively. The averaged thickness of organic shell layers ( $t_{BET}$ ) may be approximately estimated by using the  $S_{BET}$  values and the specific density of Az of 1.22,<sup>18</sup> disregarding the effect of the curvature of shell layers. The shell thickness of AzH-1, AzH-0.3 and AzH-0.1 was thus calculated to be 5.2 nm, 1.6 nm and 0.54 nm, respectively. As discussed previously, the shell thickness is not so homogeneous,<sup>25</sup> and Az nanocrystals may be filled partially in hollow spaces at joint sites of integrated silica nanoparticles so that shell layer thickness is not so uniform.

We found previously that the melting behaviour of crystals of polyaromatic compounds are markedly influenced by the nano hybridisation with silica nanoparticles.<sup>24a</sup> In this context, the existence of ultrathin shell layers of crystalline Az was indirectly deduced by calorimetric measurements. The notable feature of melting transition was found for the Az hybrids in DSC scans, as shown in Fig. 7a. The melting peak temperatures ( $T_m$ ) of the hybrids were depressed with the concurrent broadening of transition peaks, when loading amounts of Az decreases. The onset temperatures of melting were lowered considerably by the nano hybridisation. The melting started at *ca.* 38°C for AzH-0.3 and AzH-0.1. It has been well-known that the difference between melting peak temperatures of bulk and the corresponding nanoparticles ( $\Delta T_m$ ) of metals is

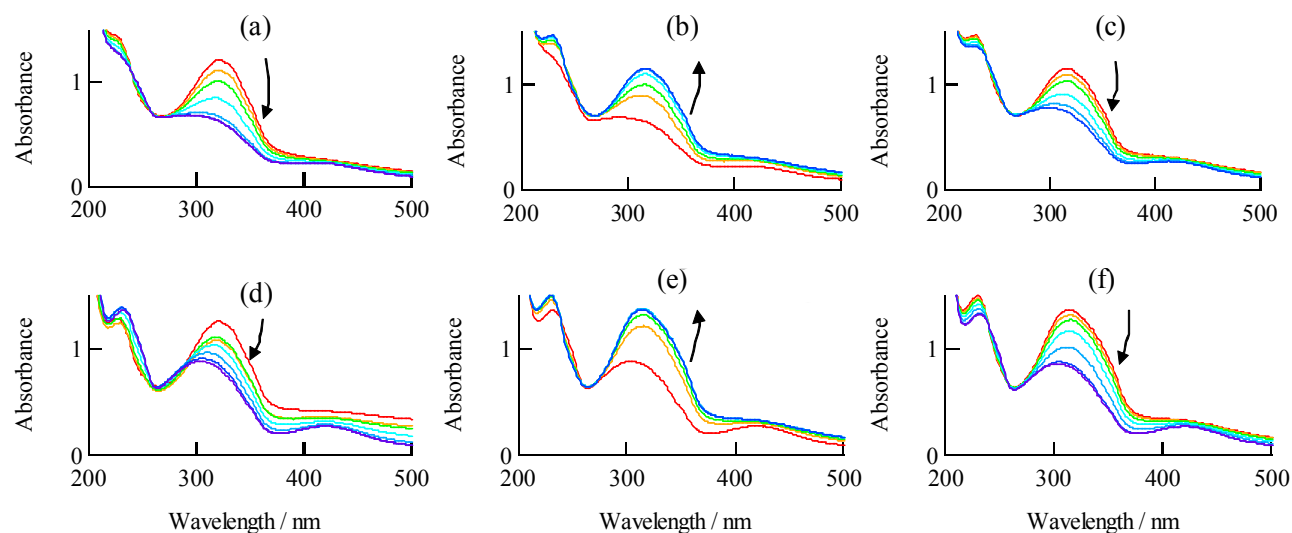


Fig. 8 Absorption spectral changes of AzH-0.046 (a-c) and AzH-0.3 (d-f) mill-dispersed in aqueous PVA solutions upon exposure to 313 nm light (a and d), subsequently to 436 nm (b and e) and to 313 nm light (c and f). The arrows indicate the alteration of the peak position during photoirradiation.

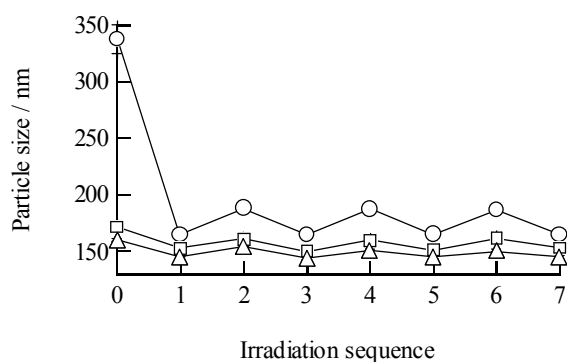


Fig. 9 Reversible changes of particles sizes of AzH-0.3 (open circles), AzH-0.1 (open squares) and AzH-0.046 (open triangles) upon alternate irradiation with 313 nm (odd sequence numbers) and 436 nm light (even sequence numbers).

inversely proportional to a particle diameter according to the classical Gibbs-Thompson equation.<sup>26</sup> The inverse proportion of  $\Delta T_m$  to organic particle sizes was confirmed in our previous study on nano-hybridised crystals of polyaromatics like phenanthrene and pyrene by employing shell layer thickness ( $t_{BET}$ ) instead of particle size. Fig. 7b shows the relationship between  $\Delta T_m$  and reciprocals of  $t_{BET}$ . Fairly good linear plots were obtained also for Az. As seen in Fig. 7b, one of the plots corresponding to AzH-1.5 deviates from the straight line, and  $T_m$  was not so markedly depressed. This may come from the insufficient hybridisation to cause the contamination with bulk crystals. The other crucial factor affected by nanocrystal size is fusion enthalpy ( $\Delta H_m$ ).<sup>26</sup> The difference in fusion enthalpy ( $\Delta\Delta H_m$ ) between those of the crystals and the hybrids was plotted against  $1/t_{BET}$ . As seen in Fig. 7c, a good linearity was obtained to confirm again. The size effect on melting transitions has been studied extensively on nanoparticles of metals<sup>27</sup> and also on organic compounds.<sup>24a,28</sup> Taking the facts into consideration, it is reasonable to assume that the Az shell layers can be treated in a kind as agglomerates of nanocrystallites.

The Az/silica hybrids (AzH-0.046, AzH-0.1 and AzH-0.3) were subjected to beads-milling in a PVA solution to prepare aqueous dispersions in the same manner as used for Az crystals. Fig. 8 shows reversible spectral changes of the aqueous dispersions of AzH-0.046 and AzH-0.3 upon the alternate exposure to 313 nm and 436 nm light. The spectral changes seem to be quite similar to those of aqueous dispersions of Az crystals, as shown in Fig. 4. Absorbances due to *E*-isomer decrease monotonously for each hybrid upon 313 nm light irradiation and recovered reversibly under illumination with 436 nm light, confirming that the photoisomerisability stems from Az molecules dissolved in PVA coils, as discussed above. No spectral crossings appeared at the longer wavelength regions due to  $n, \pi^*$ -transition because of the considerable lowering of baselines as a consequence of the formation of *Z*-isomer, implying the reversible alteration of particle sizes of the hybrids in a manner similar to that of mill-dispersed Az crystals. As shown in Fig. 9, particle sizes of AzH-0.1 and AzH-0.046 before UV irradiation is fairly larger than those after the successive irradiation with 313 nm and 436 nm light. This may be caused by relatively smaller contents of *E*-isomer at photostationary state after 436 nm light. But anomalously large decrease in particle size of AzH-0.3 after the first 313 nm light irradiation cannot be interpreted in terms of the difference in *E*-isomer fractions.

In order to shed more light on the isomerisation behaviour of mill-dispersed Az nanohybrids, the UV-VIS spectral changes were

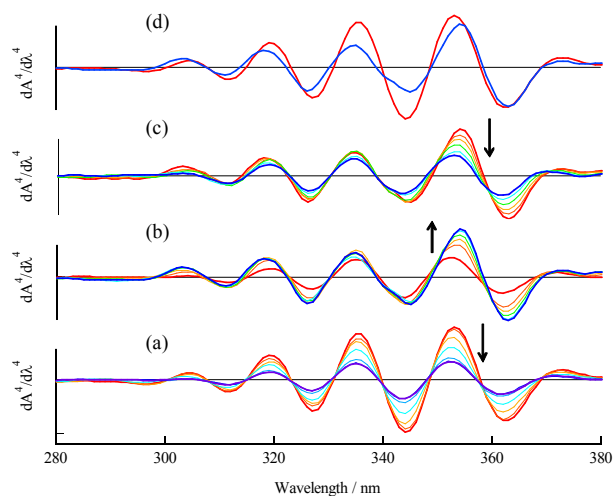


Fig. 10 Changes in the fourth derivatives of AzH-0.046 mill-dispersed in a PVA solution upon the successive exposure (a) to 313 nm, (b) 436 nm and (c) subsequently to 313 nm light and (d) the fourth derivatives before photoirradiation (red line) and after the reversion with 436 nm light irradiation (blue line).

converted into those in derivatives. Figs. 10a, 10b and 10c show the changes in the fourth derivatives of the mill-dispersed AzH-0.046 upon successive photoirradiation at 313 nm, 436 nm and again 313 nm. Apparently, common crossing points appear throughout the wavelength region for each sample to imply the involvement of *E/Z*-photoisomerisation of dissolved Az molecules as a major process. Fig. 10d shows the fourth derivatives of AzH-0.046 before photoirradiation and after the successive irradiation with 313 nm light and 436 nm light. The sub-peak positions of the regenerated *E*-isomer after the successive photoirradiation are slightly different from those of *E*-isomer of the as-prepared dispersion. The sub-peak at 353 nm before photoirradiation suffers from red shift to 355 nm, while the peaks at 319 nm and 335 nm are slightly blue-shifted. As shown in Table 1, the three sub-peaks exhibit red shift in polar solvents so that the red shift of the 353 nm peak can be interpreted in

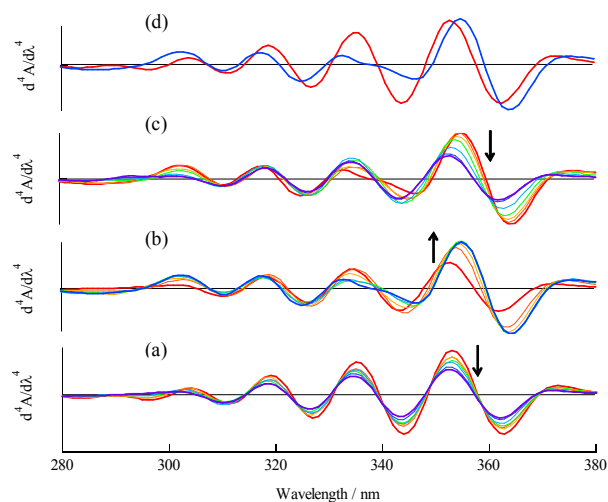


Fig. 11 Changes in the fourth derivatives of AzH-0.3 mill-dispersed in a PVA solution upon the successive exposure to (a) 313 nm, (b) 436 nm and (c) subsequently to 313 nm light and (d) the fourth derivatives before photoirradiation (red line) and after the reversion with 436 nm light irradiation (blue line).

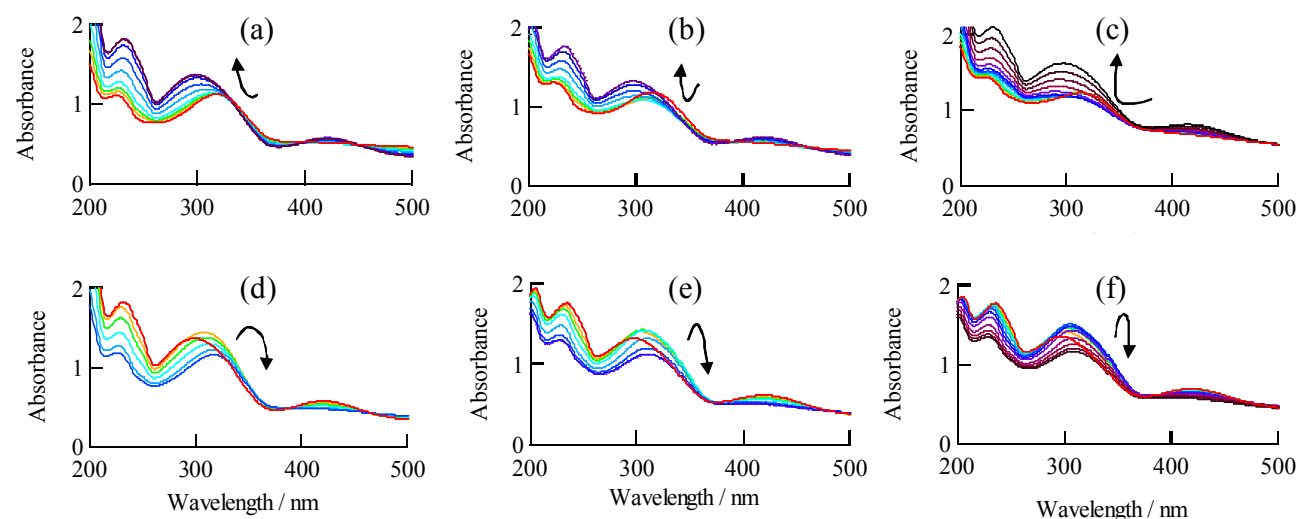


Fig. 12 Changes in absorption spectra of AzH-1 (a and d), AzH-0.3 (b and e) and AzH-0.1 (c and f) upon successive exposure to 313 nm light (a – c) and 436 nm (d – f) light. The curved arrows show the shift of the absorption peaks.

terms of the enhanced microenvironmental polarity of dissolved Az molecules as a result of *E*-to-*Z* photoisomerisation. The blue shift of the other two is assumed to be caused by the overlap with a new sub-peak probably due to a blue shifted aggregated species. This consideration is in line with the results for AzH-0.3 shown in Fig. 11. As seen in Fig. 11a for the first 313 nm light irradiation, there are many common crossing points to reveal the involvement of a single *E*-to-*Z* photoisomerisation in a way similar to the case of AzH-0.046. On the other hand, the subsequent irradiation with 436 nm light resulted in the evident deviation from common crossing points (Fig. 11 b). Moreover, as shown in Fig. 11c, when the photoirradiated dispersion was exposed again to 313 nm light, the spectral traces deviated markedly from common crossing points and become quite different from those of the first 313 nm light irradiation. The results imply the followings. First, while the first 313 nm irradiation induces a single photoisomerisation process owing to molecularly dissolved Az molecules, the concurrent occurrence of plural types of photoisomerisation is involved in photoirradiation at 436 nm and subsequently at 313 nm. Secondly, the deterioration of the singleness of photoisomerisation stems from the spectral modification of *E*-isomer. As presented in Fig. 11d, the derivative spectrum of regenerated *E*-isomer after 436 nm light irradiation is markedly dissimilar to that of as-prepared one before photoirradiation. Probably, a concentration of Az molecules incorporated in PVA coils becomes higher for AzH-0.3 when compared with AzH-0.046. Accordingly, the aggregation of dissolved *E*-isomer may be enhanced after the 436 nm photoirradiation to transform the spectral shapes, resulting in the deviation from the single photochemical process. As reported in our recent communication,<sup>14</sup> H-aggregated species with blue-shifted sub-peak was distinctly detected in the fourth order derivatives of a thin film of an LC polymer with *p*-alkoxyazobenene side chains. But the identification of H-aggregate after the 436 nm photoirradiation was unsuccessful even though the analysis with aid of much higher derivatives was attempted. Anyway, it should be mentioned that the major photoisomerisation of the hybrids dispersed in an aqueous PVA solution is due molecularly dissolved Az molecules, just as in the case of Az crystals dispersed in a PVA solution.

#### Photoisomerisation of Az hybrids dispersed in PVA-free water

In a way similar to various types of organic crystals hybridised with *m*-SiO<sub>2</sub>,<sup>24</sup> Az/silica hybrids exhibited the ability to be dispersed in water under ultrasonic treatment even in absence of dispersion stabiliser, whereas the both starting powders, *m*-SiO<sub>2</sub> and Az crystals, were unable to be dispersed homogeneously in water. We have no reasonable interpretation for such phenomenon, but this property is very convenient for our present purpose because the effect of PVA on photochemical events can be completely eliminated. After the removal of larger particles by centrifugation, aqueous dispersions of the hybrids were prepared in such a way that concentrations of Az are higher than *ca.* 10<sup>-3</sup> M to remove the contribution of Az dissolved little a bit in water at a saturated concentration of 1.7 × 10<sup>-5</sup> mol/L. The concentrations of Az in aqueous dispersions were determined by extraction with hexane. Note that a molar absorption coefficient ( $\epsilon$ ) of Az in crystalline state is extremely smaller than that in solution so that absorbances at  $\lambda_{max}$  were adjusted to be in a range from *ca.* 1 to 1.5 even though the concentrations of dispersed Az were relatively high.

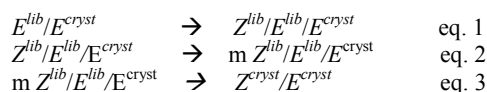
Fig. 12 summarises absorption spectral changes of aqueous PVA-free dispersions of AzH-1.0, AzH-0.3 and AzH-0.1 upon exposure to 313 nm light and the subsequent exposure to 436 nm light, respectively.<sup>15b</sup> Though  $\lambda_{max}$  before photoirradiation is centred at the wavelength of 316 nm close to that in solution, the spectral changes are extremely different from those of Az observed usually in fluid or solid solutions in the following points. First, no isosbestic point emerged, implying that more than two species participate in the photochemical processes. Secondly, absorbances at  $\lambda_{max}$  of *E*-isomer before 313 nm irradiation were smaller than those after prolonged photoirradiation generating *Z*-isomer for every hybrid, while the  $\lambda_{max}$  displayed hypsochromic shift. Thirdly, the spectral changes of *Z*-to-*E* photoisomerisation upon irradiation with 436 nm light were more complicated in such a way that absorbances at  $\lambda_{max}$  of UV-exposed dispersions increased at the early stage, followed by the reduction through the maximum, whereas  $\lambda_{max}$  exhibited a red shift (Figs. 12d, 12e and 12f). The alternate irradiation at 313 nm and 436 nm was performed to confirm the reappearance of the same spectral changes for every hybrid. In order to obtain *Z*-isomer contents at photostationary state, dispersions were extracted with hexane to obtain fourth order derivative spectra before and after 313 nm light irradiation. The *Z*-isomer contents of AzH-1 and AzH-0.1

in dispersions after prolonged UV-irradiation were 30% and 50%, respectively, and far lower than that (78%) in solution, disclosing that the *E*-to-*Z* photoisomerisation in crystalline state is discontinued.

The appearance of minimum and maximum absorbances at  $\lambda_{max}$  for the forward and backward processes, respectively, is suggestive of the involvement of consecutive reactions. Namely, while the ordinary photoisomerisation is expressed simply as  $A \rightarrow B$ , the photoisomerisation in PVA-free water may proceed according to the scheme like  $A \rightarrow B \rightarrow C$ . The EDQ-diagram is a novel procedure to know whether a process occurs through such a consecutive process.<sup>10</sup> In fact, our preliminary report presented the linearity of EDQ plots for the spectral changes of the Az nanohybrids in PVA-free dispersions, suggesting that the solid-state photoisomerisation occurs in a consecutive manner.<sup>15b</sup>

It is reasonable to assume that chemical species contributing to the anomalous spectral changes include the following three species. There may exist two types of *E*-isomer molecules in crystals according to the degree of intermolecular interactions. Az molecules at solid surfaces are liberated more or less from the confinement of crystal lattices, giving rise to the lowering of onset temperature of melting, as state above. The AFM observation of photo-induced modification of crystal surface of Az<sup>17</sup> is in line with this assumption. This type of Az molecules is denoted here as  $E^{lib}$ , whereas  $E^{cryst}$  stands for *E*-isomer molecules confined in crystal lattices and is not photoisomerisable. *Z*-isomer molecules are thought to be relatively free from the constraint of crystal lattices because of twisted conformation of phenyl rings so that the *Z*-to-*E* solid-state photoisomerisation is possible.<sup>16</sup> In this context, *Z*-isomer molecules in crystals are symbolised as  $Z^{lib}$ .

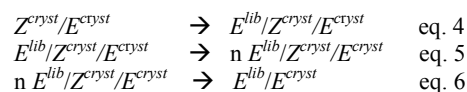
Accordingly, the following consecutive processes can be assumed to occur during 313 nm light irradiation. The initial step (eq. 1) consists of the photoisomerisation of *E*-isomer molecules at the uppermost shell surfaces.<sup>17</sup>  $E^{lib}/E^{cryst}$  in eq. 1 expresses the coexistence of liberated and restrained *E*-isomer molecules at a surface region, while the slash stands for the borderline between the two types of molecules. The UV-induced conversion of  $E^{lib}$  into  $Z^{lib}$  generates a front line comprised of new  $E^{lib}$  because the constraint of *E*-isomer molecule between  $Z^{lib}$  and  $E^{cryst}$  is reduced.  $Z^{lib}/E^{lib}/E^{cryst}$  in eq. 1 expresses such situation. Subsequently, the  $E^{lib}$  at the borderline becomes photoisomerisable so that the further *E*-to-*Z* photoisomerisation is possible. This process is expressed as eq. 2. As described above, the solid state *E*-to-*Z* photoisomerisation is actually brought to a halt. This may be caused by the crystallisation of *Z*-isomer ( $Z^{cryst}$ ) after a threshold number (*m*) of  $Z^{lib}$  is formed, as expressed as eq. 3.



On the basis of the mechanism proposed here, the increment of absorbances at  $\lambda_{max}$  through the minima during *E*-to-*Z* photoisomerisation can be interpreted in terms of difference in  $\epsilon$  of the three kinds of species. It is likely that  $\epsilon$  of  $E^{cryst}$  is far smaller than that of  $E^{lib}$  due to strong molecular interactions. This was actually confirmed by extracting Az crystals in an aqueous dispersion with hexane to estimate  $\epsilon$  of Az in crystals. Meanwhile, intermolecular interactions of *Z*-isomer are inherently so small because of the bent molecular shape that  $\epsilon$  of *Z*-isomer molecules is practically not influenced by the location in crystals. In other words,  $\epsilon$  of  $Z^{lib}$  is close to that of  $Z^{cryst}$ . Accordingly, the amplitude of  $\epsilon$  is considered to be in the following order;  $E^{lib} > Z^{lib} \approx Z^{cryst} > E^{cryst}$ . The first step (eq. 1) leads to the slight decrease of absorbances at  $\lambda_{max}$  because of the consumption of molecules at surface region denoted

as  $E^{lib}$ . Further illumination with 313 nm light leads to the second process (eq. 2) to result in the increment of absorbances of blue-shifted  $\lambda_{max}$  because of the accumulation of  $Z^{lib}$ , giving rise to the absorbance minima, as shown in Figs 12a, 12b and 12c.

The spectral traces during the backward photoisomerisation can be interpreted in terms of two factors. The first is the difference in  $\epsilon$  of the three species, as mentioned above. The second is related with the crystallisation of as-formed *E*-isomer ( $E^{lib}$ ). The first step upon exposure to 436 nm light is the conversion of  $Z^{cryst}$  into as-formed  $E^{lib}$  as shown in eq. 4. As a result, absorbances at  $\lambda_{max}$  hike at the early stage owing to the largest  $\epsilon$  of  $E^{lib}$ . The accumulation of  $E^{lib}$  molecules leads to the crystallisation at a critical concentration to give  $E^{cryst}$ , as expressed in eq. 5. Because of the smallest  $\epsilon$  of  $E^{cryst}$ , the second process displays the considerable decrease in absorbance through the maximum. Since *Z*-isomer is photoisomerisable even in crystalline state,<sup>16</sup> the second process continues until the complete consumption of *Z*-isomer to regenerate crystalline *E*-isomer according to eq. 6.



In order to verify the validity of the mechanism proposed above, changes in absorption spectra shown in Fig. 12 were converted into those in the fourth order derivatives. Fig. 13 shows changes in the fourth derivatives upon exposure to 313 nm light. As opposed to the events in solution (Fig. 1c) and in an aqueous milled-dispersion in PVA solution (Fig. 4b), quite different behaviour was observed and summarised as follows. First, the fine structure assignable to VLT of  $\pi, \pi^*$ -band of Az before photoirradiation does not emerge in the 300 nm ~ 350 nm region because of strong intermolecular interactions in crystal lattices. Secondly, the UV-irradiation gives rise to very feeble alteration of  $d^4$  at ca. 350 nm owing to low sub-peak height, reflecting the broad  $\pi, \pi^*$ -band in crystals. Thirdly, the notable growth of  $d^4$  is induced at 275 nm. This sub-peak is evidently assignable to *Z*-isomer. The slight increment of  $d^4$  at 298 nm arises also from the formation of *Z*-isomer. When compared with  $\lambda_{max}$  of *Z*-isomer at 249 nm in solution (Fig. 1), the  $\lambda_{max}$  at 275 nm is markedly red-shifted probably because of intermolecular interactions. Remind here that the changes in absorption spectra shown in Fig. 12 cannot offer such detailed information concerning *Z*-isomer.

Fig. 14 shows changes in the fourth derivatives during the

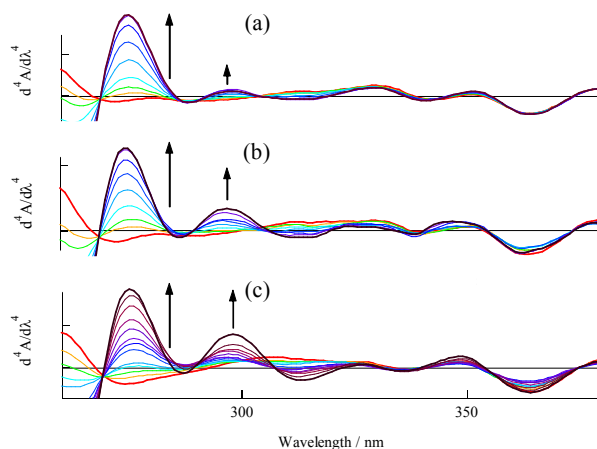


Fig. 13 Changes in the fourth derivatives of aqueous PVA free dispersions of (a) AzH-1.0, (b) AzH-0.3 and (c) AzH-0.1 upon exposure to 313 nm light.

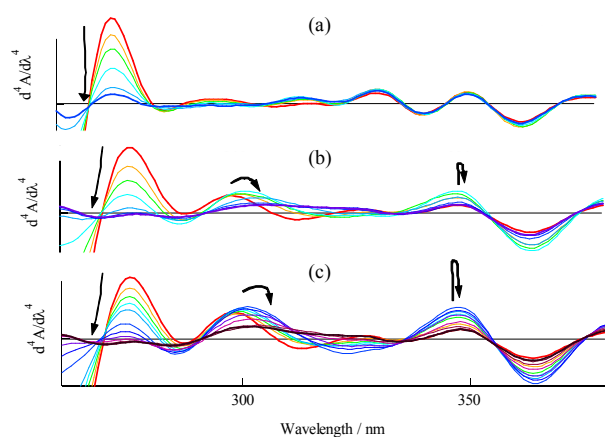


Fig. 14 Changes in the fourth derivatives of aqueous PVA-free dispersions of (a) AzH-1.0, (b) AzH-0.3 and (c) AzH-0.1 upon exposure to 436 nm light. The arrows indicate the alteration of the peak position.

subsequent irradiation with 436 nm light, and the characteristic features are summarised as follows. First, the sub-peak due to *Z*-isomer at 275 nm declines smoothly because of the backward photoisomerisation. Secondly, the spectral changes in the region of 290 nm ~ 340 nm are complicated particularly for AzH-0.3 and AzH-0.1. As illustrated by the curved arrows drawn in Fig. 14,  $d^4$  of the sub-peak at 298 nm increases at the early stage, followed by the decrement through the maximum, while the wavelengths of the sub-peak suffer from blue shift to reach finally to that of *E*-isomer. This sort of phenomenon is suggestive of the partial overlapping of sub-peaks of both isomers in this wavelength region. Thirdly, the peak at 348 nm of AzH-0.3 and AzH-0.1 grows at first, followed by the decline through the maximum without the modification of the peak position. Since the peak at 348 nm is exclusively due to *E*-isomer, it is evident that two types of species of *E*-isomer, i.e.  $E^{cryst}$  and  $E^{lib}$ , participate in this sort of curious changes in  $d^4$ . In other words, the transient formation of  $E^{lib}$  plays an essential role in generating the spectroscopic features of the solid-state photoisomerisation.

Based on the discussion on the results shown in Figs. 13 and 14, it is reasonable to claim that the individual photoisomerisation of *E*- and *Z*-isomer is monitored by following changes in  $d^4$  at 348 nm and 275 nm, respectively, as a function of exposure doses. The results are summarised in Fig. 15, where  $d^4$  values are normalised. As seen in Fig. 15a for 313 nm light photochemistry, the fluctuation of  $d^4$  at

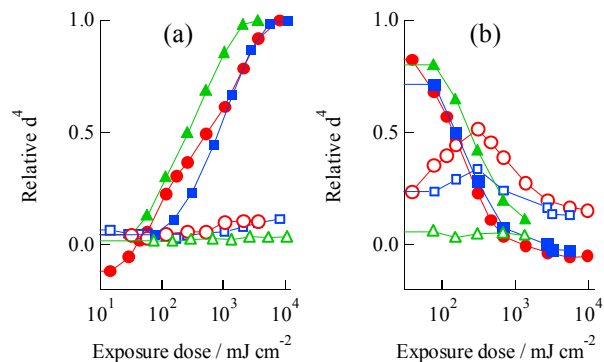


Fig. 15 Changes in relative  $d^4$  values of aqueous PVA-free dispersions of AzH-1.0 (blue squares), AzH-0.3 (green triangles) and AzH-0.1 (red circles) at 275 nm (closed marks) and 348 nm (open marks), respectively, as a function of exposure doses of (a) 313 nm and (b) 436 nm light.

348 nm for each sample is so small that detailed information about *E*-to-*Z* photoisomerisation is hardly available. Besides, the difference in  $d^4$  at 348 nm before and after 313 nm light irradiation is not evident, whereas the UV-irradiation should lead to the reduction of the  $d^4$  because of the consumption of *E*-isomer. This may be due to the fact that the difference in the  $d^4$  values before and after the photoirradiation falls within instrumental errors. Concerning the increment of  $d^4$  at 275 nm assignable to *Z*-isomer, the values hike approximately linearly against logarithmical exposure doses to be saturated at doses of 3 ~ 5 J cm<sup>-2</sup>. Such exposure doses are not far from those needed to reach at a photostationary state for the solid-state *E*-to-*Z* photoisomerisation of Az crystals mill-dispersed in aqueous PVA solutions (Fig. 5). And the result is also in line with eq. 3 expressing the crystallisation of *Z*-isomer to bring a halt of photoisomerisation.

As presented in Fig. 15b, the subsequent 436 nm light irradiation brings about the approximately linear decrease in  $d^4$  at 275 nm owing to *Z*-to-*E* photoisomerisation, which is levelled off at ca. 1 J cm<sup>-2</sup> dose for every hybrid. The remarkable feature is observed for the changes in  $d^4$  at 348 nm for AzH-0.3 and AzH-0.1, respectively. There exists the  $d^4$  maximum at a dose of ca. 400 mJ cm<sup>-2</sup>, and  $d^4$  declines subsequently upon further blue light irradiation. This kind of unique behaviour can be reasonably interpreted on the basis of the consecutive processes expressed as eqs. 4 and 5 in accordance with the discussion mentioned above. As stated before,  $\epsilon$  of  $E^{lib}$  is the largest so that  $d^4$  grows as a result of *Z*-to-*E* photoisomerisation according to eq. 4. Afterwards, the crystallisation of  $E^{lib}$  takes place at a critical concentration according to the subsequent process (eq. 5), leading to the decline of  $d^4$ . It is worthy to note that the sub-peak position at 347 nm is essentially not altered throughout the blue light irradiation, suggesting that the wavelength at 347 nm is not affected by whether *E*-isomer exists as  $E^{lib}$  or  $E^{cryst}$ . In short, the appearance of the maximum in the spectral changes shown in Figs. 12d ~ 12f stems from the generation and the subsequent crystallisation of transient  $E^{lib}$ .

## Experimentals

### Materials

Az was purchased from Tokyo Kasei and used as received. The surface-modified silica nanopowder (m-SiO<sub>2</sub>) of primary mean diameter of 14.1 nm was donated by Toda Kogyo Co., Ltd. The PVA of saponification degree of 88% and polymerisation degree of 500 (Nippon Gosei; GL-05) was gifted by Murakami Co. Ltd.

### Beads milling of Az in a PVA solution

The wet beads milling was achieved by using a planetary mill (Fritsch; P-7) installed with a couple of zirconia vessels (25 mL). Az crystals (150 mg) were added to 10 mL of a 5 wt% solution of the PVA placed in each vessel and milled with aid of zirconia beads of  $\phi = 0.1$  mm as a milling agent at a rotation speed of 600 rpm for 1 hr. The beads were removed by filtration to obtain an aqueous dispersion. Aqueous dispersions of Az/m-SiO<sub>2</sub> hybrid powders were prepared in the same way.

### Preparation of Az/m-SiO<sub>2</sub> hybrid powders

A mixture of Az crystals and m-SiO<sub>2</sub> (total weight = 1 ~ 2 g) were ground in a mortar in advance and placed in zirconia vessels. The dry milling was carried out with aid of nylon beads of  $\phi = 4$  mm at a rotation speed of 300 rpm for 1 hr, followed by removing the beads to obtain voluminous hybrid powders.

### Wet milling of Az/m-SiO<sub>2</sub> hybrids in an aqueous PVA solution

Powdery hybrid (150 mg) suspended in 10 mL of a 5 wt% aqueous solution of GL-05 and milled with aid of zirconia beads of  $\phi = 0.1$  mm at a rotation speed of 600 rpm for 1 hr, followed by centrifugation at 3500 rpm for 10 min to remove crude particles.

### Preparation of PVA-free dispersion of Az/SiO<sub>2</sub> hybrids

Powdery hybrid (100 mg) was suspended in 5 mL deionised water and subjected to ultrasonic treatment for 20 min, followed by centrifugation at 3500 rpm to remove crude particles.

### Photoirradiation

A solution or an aqueous dispersion in a quartz cuvette was irradiated under magnetic stirring with actinic light from a 500 W super-high pressure mercury passed through suitable filter combinations to select monochromatic light of 313 nm and 436 nm, respectively. UV spectral measurements were performed at intervals to follow the reaction.

### Physical measurements

Absorption spectra were taken on a diode array spectrometer (Shimadzu; Multistep 1500) at 1 nm spacing. Absorbances of solutions as well as aqueous dispersions were adjusted to be in the range of *ca.* 0.8 ~ 1.2. The spectra were normalised in such a way that absorbances at  $\lambda_{max}$  were equal to 1, followed by the differentiation and smoothing according to the Savitzky-Golay algorithm, for the convenience of analysing absorption as well as derivative spectra. The extraction of Az from aqueous dispersions was carried out as follows. One mL of an aqueous dispersion was shaken with 5 mL of hexane in a capped test tube, followed by removing an aqueous layer and drying an organic layer over magnesium sulphate. A dried solution was diluted five times with hexane to take an absorption spectrum. Particle sizes of dispersions were measured by means of dynamic light scattering (Malvern; Nano-Z).

### Conclusion

The usefulness of higher order derivative spectra is stressed by their application to reveal the photoisomerisation behaviour of Az in heterogeneous systems. The conclusive remarks are summarised as follows.

(1) Changes in derivatives spectra of Az in solution upon photoirradiation exhibit many common crossing points to confirm the involvement of a single process without any side reaction. Accordingly, derivative spectra go beyond absorption spectra to determine the unity of a reaction, since isosbestic points are sometimes not clearly observed in absorption spectral changes. Besides, the positions of VLT sub-peaks in higher order derivatives of *E*-isomer are far from those of *Z*-isomer so that the photoisomerisation in solution is followed simply by monitoring changes in  $d^4$  values of VLT sub-peaks.

(2) Higher order derivative spectra revealed that reversible absorption-spectral changes of an aqueous dispersion of Az crystals beads-milled in a PVA solution were indistinguishable from solution photochemistry due to the partial dissolution of Az in aqueous PVA solutions. The fast *E-to-Z* conversion due to dissolved Az was about 14 % and followed by about one order magnitude slower solid-state photoisomerisation. Particle sizes of mill-dispersed crystalline Az were reversibly altered upon alternate exposure to 313 nm and 436 nm. This phenomenon was interpreted in terms of reversible changes of dipole-dipole interactions of Az molecules incorporated in PVA chains which cover surfaces of Az particles to stabilise the dispersion.

(3) Core-shell type powdery nanohybrids provided by the dry milling of mixtures of Az crystals and m-SiO<sub>2</sub> served the fabrication of two types of aqueous dispersions of Az. The first was aqueous dispersions prepared by the wet milling in aqueous PVA solution, whereas the second was PVA-free aqueous dispersions prepared by the ultrasonic treatment in water. The performances of the former including photoisomerisation and particle size changes were essentially

identical to those of Az milled in PVA solutions because of the incorporation of Az molecules in PVA chains. On the contrary, PVA-free dispersions exhibited exceptional spectral changes upon photoirradiation, suggesting that both of *E-to-Z* and *Z-to-E* photoisomerisations in crystalline state takes place in a successive manner owing to the participation of three kinds of species; restrained *E*-isomer ( $E^{cryst}$ ), librated *E*-isomer ( $E^{lib}$ ) and *Z*-isomer ( $Z^{lib}$ ). The analysis of higher derivative spectra led to the conclusion that the solid-state *E-to-Z* photoisomerisation is kicked off from *E*-isomer molecules at the topmost crystal surface through the processes expressed as  $E^{lib}/E^{cryst} \rightarrow m Z^{lib}/E^{lib}/E^{cryst} \rightarrow n Z^{cryst}/E^{cryst}$ , whereas the slashes stand for boundary regions. The *Z-to-E* reversion proceeds through the processes denoted as  $Z^{cryst}/E^{cryst} \rightarrow E^{lib}/Z^{cryst}/E^{cryst} \rightarrow E^{lib}/E^{cryst}$ . Consequently, the unique changes in absorption spectra of the PVA-free dispersions originate from the marked difference in  $\epsilon$  between  $E^{dis}$  and  $E^{cryst}$ .

The present results encourage us to analyse photochemical reactions occurring in versatile matrices including crystalline states by means of higher order derivative spectra, because they provide far more valuable information when compared with fundamental UV-VIS absorption spectra.

### Acknowledgement

The author is indebted to Faculty of Science, Toho University for financial support. He thanks to Dr. Haruhisa Akiyama for his DSC measurements and Mr. Shinji Horie of Toda Industry Co. Ltd. for his contribution to BET measurements.

### Notes and references

† The experimental works were carried out in 2008-2009 at Faculty of Science, Toho University, 2-2-1 Miyama, Funabashi, Chiba 274-8510, Japan.

<sup>a</sup> Present address: R & D Centre, Murakami Co. Ltd., 1-6-12 Ohnodai, Midori-ku, Chiba 267-0056, Japan. E-mail: k\_ichimura@murakami.co.jp.

- H. M. D. Bandara and S. C. Burdette, *Chem. Soc. Rev.*, 2012, **41**, 1809 (references are cited therein).
- a) R. H. El Halabieh, O. Mermut and C. J. Barrett, *Pure Appl. Chem.*, 2004, **76**, 1445; b) E. Merino, *Chem. Soc. Rev.*, **40**, 3835 (2011); E. Merino and M. Ribagorda, *Beilstein J. Org. Chem.* 2012, **8**, 1071.
- a) Z. Sekkat and W. Knoll eds. *Photoreactive Organic Thin Films*, Academic Press, 2002; b) Y. Zhao and T. Ikeda eds., *Smart Light-Responsive Materials: Azobenzene-containing Polymer and Liquid Crystals*, A John Wiley & Sons Ltd, New Jersey, 2009.
- a) K. Ichimura, *Chem. Rev.* 2000, **100**, 1847; b) V. G. Chigrinov, V. M. Kozenkov and H. -S. Kwok, *Photoalignment of Liquid Crystalline Materials: Physics and Applications*, John Wiley & Sons Ltd, West Sussex, 2008; c) T. Seki, S. Nagano and M. Hara, *Polymer*, 2013, **54**, 6053.
- T. Ube and T. Ikeda, *Angew. Chem. Int. Ed.*, 2014, **53**, 10290.
- A. Natansohn and P. Rochon, *Chem. Rev.* 2002, **102**, 4139.
- R. Hagen and T. Bieringer, *Adv. Mater.*, 2001, **13**, 1805
- K. Ichimura, N. Fukushima, M. Fujimaki, S. Kawahara, Y. Matsuzawa, Y. Hayashi and K. Kudo, *Langmuir*, 1998, **25**, 6780.
- M. Ueda, N. Fukushima, K. Kudo and K. Ichimura, *J. Mater. Chem.*, 1997, **7**, 641.
- a) G. Quinkert, *Angew. Chem., Int. Ed.*, 1972, **11**, 1072; b) G. Gauglitz, *Photochromism – Molecules and Systems*, ed. H. Dürr and H. Bouas-Laurent, Elsevier, Amsterdam, 1990, p. 15; c) K. Ichimura and S. Watanabe, *Bull. Chem. Soc. Jpn.*, 1976, **49**, 2224.
- (a) G. Talsky, L. Mayring and H. Kreuzer, *Angew. Chem., Int. Ed.*, 1978, **17**, 785; (b) J. Karpinska, *Talanta*, 2004, **64**, 801; (c) F. S. Rojas and C. B. Ojeda, *Anal. Chim. Acta*, 2009, **635**, 22.
- K. Ichimura, S. Iwata, S. Mochizuki, M. Ohmi and D. Adachi, *J. Polym. Sci. Part A Polym. Chem.*, 2012, **50**, 4094.
- K. Ichimura, *J. Mater. Chem. C*, 2014, **2**, 641.

14. K. Ichimura and S. Nagano, *RSC Adv.*, 2014, **4**, 52379.
15. As preliminary reports: a) K. Ichimura, *Chem. Commun.*, 2009, 1496; b) K. Ichimura, *Chem. Commun.*, 2010, **46**, 3295.
16. G. S. Hartley, *Nature*, 1937, **14**, 281.
17. K. Nakayama, L. Jiang, T. Iyoda, K. Hashimoto and A. Fujishima, *Jpn. J. Appl. Phys., Part 1*, 1997, **36**, 3898.
18. C. J. Brown, *Acta Crystallogr.*, 1966, **21**, 146.
19. A. Mostad and C. Romming, *Acta Chem. Scand.*, 1971, **25**, 3561.
20. a) T. Ikeda, J. Mamiya and Y. Yu, *Angew. Chem., Int. Ed.*, 2007, **46**, 506; b) M. Yamada, M. Kondo, R. Miyasato, Y. Naka, J. Mamiya, M. Kinoshita, A. Shishido, Y. Yu, C. J. Barrett and T. Ikeda, *J. Mater. Chem.*, 2009, **19**, 60; reference therein.
21. S. Tanaka, H.-K. Kim, A. Sudo, H. Nishida, T. Endo, *Macromol. Chem. Phys.*, 2008, **209**, 2071; references therein.
22. M. Irie and T. Suzuki, *Makromol. Rapid Comm.*, 1987, **8**, 607.
23. K. Hayashi, H. Morii, K. Iwasaki, S. Horie, N. Horiishi and K. Ichimura, *J. Mater. Chem.*, 2007, **17**, 527.
24. a) K. Ichimura, K. Aoki, H. Akiyama, S. Horiuchi, S. Nagano and S. Horie, *J. Mater. Chem.*, 2010, **20**, 4312; b) K. Ichimura, A. Funabiki and K. Aoki, *Chem. Lett.*, 2010, **39**, 586; c) K. Ichimura, *Chem. Lett.*, 2010, **39**, 614; d) A. Funabiki, T. Mochida, H. Hasegawa, K. Ichimura and S. Kimura, *New J. Chem.*, 2011, **35**, 483; e) K. Ichimura, *Phys. Chem. Chem. Phys.*, 2011, **13**, 5974; f) A. Funabiki, H. Sugiyama, T. Mochida, K. Ichimura, T. Okubo, K. Furukawa and T. Nakamura, *RSC Adv.*, 2012, **2**, 1055.
25. S. Horiuchi, S. Horie and K. Ichimura, *ACS Appl. Mater. Interfaces*, 2009, **1**, 977.
26. J. Sun and S. L. Simon, *Thermochim. Acta*, 2007, **463**, 32.
27. (a) M. Takagi, *J. Phys. Soc. Jpn*, 1954, **9**, 359. b) "Metal Nanoparticles: Synthesis, Characterization and Applications," ed. D. L. Feldheim and C. A. Foss, Jr., Marcel Dekker, New York and Basel, 2002; (c) V. Rotello, "Nanoparticles: Building Blocks for Nanotechnology," Springer, New York, 2003; (d) "Nanoparticles: from Theory to Application," ed. Günter Schmid, Wiley-VCH, Weinheim, 2004; (e) "Nanoparticle Technology Handbook," ed. M. Hosokawa, K. Nogi, M. Naito and T. Yokoyama, Elsevier, Amsterdam, 2007.
28. (a) C. L. Jackson and G. B. McKenna, *J. Chem. Phys.*, 1990, **93**, 9002; (b) R. Mu and V. M. Malhotra, *Phys. Rev. B*, 1991, **44**, 4296; (c) C. L. Jackson and G. B. McKenna, *Chem. Mater.*, 1996, **8**, 2128; d) J.-M. Ha, M. A. Hillmyer and M. D. Ward, *J. Phys. Chem. B*, 2005, **109**, 1392.